Anomalous self-assembly of gelatin in ethanol-water marginal solvent

H. B. Bohidar* and B. Mohanty
School of Physical Sciences, Jawaharlal Nehru University, New Delhi-110067, India
(Received 25 November 2002; revised manuscript received 16 July 2003; published 19 February 2004)

Light scattering, rheology, and atomic force microscope (AFM) studies have been performed on solutions of a polyampholyte (gelatin) prepared in water-ethanol marginal solvent. At ethanol concentration $\approx 45 \pm 2\%$ v/v anomalous aggregation led to formation of fractal (on hydrophilic substrates; glass, quartz and silicon) aggregate of polypeptide molecules having fractal dimension d_f in $2D = 1.60 \pm 0.08$. The time evolution morphology of these self-assembled and self-organized structures formed on hydrophilic substrates was driven by selective ethanol evaporation and was observed by an AFM. These fractal aggregates eventually transformed into near-spherical clusters with fractal corona having same fractal dimension ($d_f = 1.58 \pm 0.05$) and finally, the corona separated and regular aggregates were formed. The kinetics of aggregation on substrates could be modeled through random sequential adsorption of particles with continuum power-law size distribution. The temporal growth of aggregate hydrodynamic radius $R_h(t)$ and scattered intensity $I_s(t)$ measured in the bulk were observed to exhibit; $R_h \sim t^z$ and $I_s \sim t^z$-with $z = 1/d_f$, giving a fractal dimension d_f in $3D \approx 2.6 \pm 0.2$, which is discussed within the framework of Smoluchowski aggregation kinetics. This growth in R_h is accompanied by narrowing down of the particle size distribution. Solution rheology at this ethanol concentration revealed minimum thixotropy and maximum infinite shear viscosity features.

DOI: 10.1103/PhysRevE.69.021902 PACS number(s): 87.14.Ee, 05.70.Ln, 82.70.Gg, 87.15.He

I. INTRODUCTION

The phenomenon of aggregation is of significant interest to biology, immunology, polymer science, colloidal chemistry, metallurgy, and nucleation processes close to phase transitions. Such aggregations in polyelectrolytic solutions produce polymer-rich solvated condensates, called coacervates that have rich biological implications [1,2]. Self-organization and aggregation processes have been described through diffusion limited cluster aggregation (DLA) [3], reaction limited cluster aggregation (RLA) [4], random sequential adsorption (RSA) [5,6], etc. The quantification of these aggregates is done through the Hausdorff mass fractal dimension d_f, which is much smaller than the corresponding Eucleadian dimension (D). In this picture, the density-density correlation function, $g(r) = \langle \rho(r)\rho(0) \rangle \sim r^{-A}$, where $A = D - d_f$. Diffusion driven processes rapidly coagulate to yield DLA clusters of fractal dimension, $d_f \cong 1.7$ for $D = 2$ and 2.6 for $D = 3$ which is strongly supported by simulations and experimental results [6]. On the other hand RLA clusters grow rather slowly because of reduced collision probability between particles and the growth is through interparticle reactivity involving equilibrium constant. The corresponding fractal dimensions are much higher than that of DLA clusters. Though the crossover from DLA to RSA has been observed, the intermediate region remains relatively unexplored [7].

Adhesion of macromolecules onto surfaces, polymer chain reactions, association of noncrystalline granular materials and arrangement of nanostructures, quantum memory devices, biosensors on substrates, car parking, etc. fall in to the category of a random sequential adsorption process. These processes are generated with sequential addition of particles at a constant rate to a substrate where overlapping and leaving the cluster once a part is forbidden. Brilliantov *et al.* [8] have shown that geometric and kinetic features of the RSA clusters for a system showing polydispersity in size are governed by the smallest size particles but prior to this an intermediate asymptotic regime prevails.

Gelatin, a polyampholyte obtained from denatured collagen, is a polypeptide and is an ideal case for such studies. Aqueous solutions properties of gelatin have been well studied and characterized in the past [9,10]. Depending on the process of recovery the gelatin molecules bear different physical characteristics. Type-A gelatin is acid processed, has an isoelectric pH, pI$\approx$9 whereas the alkali processed type-B gelatin has pI$\approx$5 [11]. The monomeric representation of this polypeptide is $(\text{Gly-}X\text{-Pro})_n$, where X is an amino acid. The detailed chemical composition of this biopolymer is as follows (as per Merck index): Glycine constitutes 26%, alanine and arginine are in a 1:1 ratio together constitute $\approx$20%, proline is $\approx$14%, glutamic acid and hydroxyproline are in a 1:1 ratio constituting $\approx$22%, aspartic acid $\approx$6%, lysine $\approx$5%, valine, leucine, and serine constitute $\approx$2.0% each, rest 1% is comprised of isoleucine and threonine, etc. In the past all the coacervation studies on gelatin involved complexation between type A and type B, or gelatin and acacia molecules [12,13].

The present work uses an array of experimental techniques to study self-association phenomenon of type-B gelatin (a low charge density biomolecule) in a marginal ethanol-water solvent close to the isoelectric pH of the protein. This self-assembly was observed in a very narrow range of ethanol concentration. No such study has ever been undertaken despite the fact that such an understanding may serve as a precursor to the mapping of the complexities of biopolymeric self-organization as a whole. Though multivalent salt induced complexation of gelatin has been reported in the past [14], the universality of surface adsorbed growth dy-

*Corresponding author. Email address: bohi0700@mail.jnu.ac.in

namics of this biopolymer where aggregation is driven by dehydration of the gelatin molecules was never established conclusively, which is the main objective of this paper. In addition, we study the time-dependent aggregation in the bulk of the solution and the solution rheological properties in an attempt to understand this anomalous aggregation phenomenon. In this paper, we first look at the two-dimensional (2D) behavior of gelatin aggregates, and next move to see the 3D features (aggregation in bulk) and to seek the answer to the anomalous self-assembly; we probe (through rheology) the role of hydrogen bonding [15].

II. MATERIALS AND METHODS

Ethanol was obtained from Merck, Germany. Gelatin (Type B, microbiology grade devoid of E. Coli and liquifier presence) and sodium chloride were bought from E. Merck, India. The gelatin sample was bovine skin extract, and the bloom strength was 75 and had a molecular weight $\approx(90 \pm 10)$ kDa determined from SDS/PAGE. All other chemicals used were bought from Thomas Baker, India. All the chemicals were of analytical grade. The gelatin samples were used as supplied. The solvent used was deionized water, pH (using 0.1*M* HCl or 0.1*M* NaOH), and the ionic strength of the solvent was first set as per the experimental requirement (0.1*M* NaCl) and the gelatin solutions (1% w/v) were prepared by dispersing gelatin in this medium at 60 °C and the pH set to 5.01. The macromolecules were allowed to hydrate completely, this took 30 min to 1 h. The final stock solution was a transparent liquid. The gelation concentration of gelatin in water is $\approx 2\%$ (w/v), the gelatin concentration chosen in these experiments was deliberately kept lower than this to avoid the formation of gels. Samples were checked at various stages by passing these through SDS/PAGE to ensure absence of gelatin degradation.

The time dependent particle sizing measurements were done by the dynamic laser light scattering (DLS) technique, using a Brookhaven-9000AT digital autocorrelator (Brookhaven Instruments, USA) and a homemade goniometer. The excitation source was a diode pumped solid state laser (Model-DPY 305-II, Adlas, Germany) emitting 50 mW of power at 532 nm in linearly polarized single frequency mode. The scattering angle was fixed at 90° and the data analysis was done using CONTIN software provided by Brookhaven Instruments. More on DLS and data analysis can be found elsewhere [16]. During the course of size measurements the intensity of the scattered light was monitored continuously as a function of time over a period of 12 h.

During the experiment, a drop of the solution was removed from the reaction beaker and allowed to spread out uniformly on a degreased glass cover-slip plate over a period of 20 to 30 min. Atomic force microscope (AFM) pictures were taken using a Autoprobe CP Research AFM system, model AP-2001 (Thermomicroscopes, USA) using a 90-μm scanner and a tapping mode. These experiments were repeated with the gelatin sample (type B) resourced from Sigma chemicals (a bloom of 75) and for each of these two samples four different substrates were chosen, namely, glass, quartz, silicon, and mica.

The rheology experiments were performed using a AR-500 stress controlled rheometer (T. A. Instruments, UK). The steady state shear flow and dynamic rheology of the solutions were studied using a cone plate geometry of radius 60 mm and angle 2°. Appropriate inertial corrections were made prior to accepting data. Sponges were used as solvent trap to prevent loss of solvent due to evaporation. Thixotropic measurements were performed (in flow mode) on water-ethanol and water-ethanol-gelatin system at ethanol concentration fixed at $45\pm 2\%$ v/v. In this procedure, starting at the lowest shear rate ($\dot{\gamma}$) available, one obtains the shear stress (σ) developed in the system. After a given time, the shear rate is increased to its next higher value and shear stress measured again. This is repeated until the highest shear rate is reached and the system is sheared to its equilibrium shear stress. The process is reversed in the next step. The shear rate is reduced stepwise and stress measured continuously until the minimum shear rate is reached. A plot of shear stress as function of shear rate reveals the thixotropic behavior of the system.

III. RESULTS AND DISCUSSIONS

A. Random sequential adsorption and transient morphology of aggregates

These processes are generated with sequential addition of particles at a constant rate to a substrate where overlapping and leaving the cluster, once apart, is forbidden. Brilliantov *et al.* [7] have shown that geometric and kinetic features of the RSA clusters for a system showing polydispersity in size are governed by the smallest size particles, but prior to this an intermediate asymptotic regime prevails. Brilliantov *et al.* [8] assumed the particle size distribution to be continuous and represented it as a power-law distribution function $P(R)$ given by

$$P(R)=\begin{cases} \alpha R^{\alpha-1}, & R\leqslant R_{\max} \\ 0, & R>R_{\max}. \end{cases} \tag{1}$$

The system is assumed to have very large polydispersity in size with the maximum size given by $R_{\max}$. The geometrical structure of the resultant RSA cluster evolving from a system with characteristics defined by particle size distribution as in Eq. (1) is fully governed by the spatial correlations inside the system, which is accounted for by the parameter α $(\alpha>0)$. As α increases from 0 to ∞, d_f reduces from 2 to 1.305. For smaller α fractal clusters are formed while the Apollonian packing limit is reached as $\alpha\rightarrow\infty$. If $n(R)$ is the number of adsorbed particles per unit area, it can be shown that [8]

$$n(R)\sim R^{\alpha-1+(z+1)/v}. \tag{2}$$

In the RSA formalism, as the particles are added sequentially the fraction of the uncovered area decreases with time t, following the power-law $\sim t^{-z}$, which results in the reduction of the typical gap between two neighboring adsorbed particles following the power law $\sim t^{-v}$. One gets the fractal dimension of the resultant cluster as [8]

$$d_f=D-z(D+\alpha). \tag{3}$$

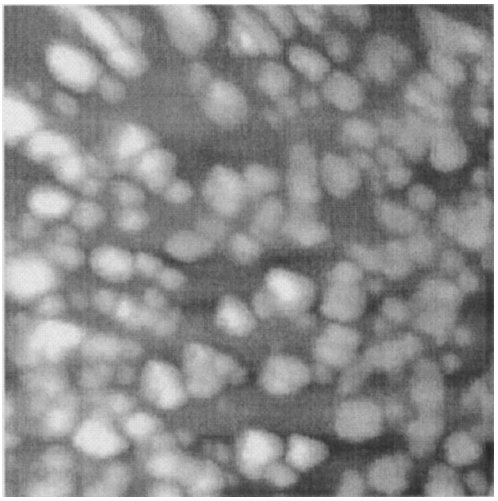

FIG. 1. Scanning probe micrograph (5×5 μm^2) of a 1% w/v aqueous gelatin solution with 0.1*M* NaCl taken at 25 °C in the tapping mode. The picture shows gelatin aggregates of sizes 65 nm, 190 nm, 380 nm, and larger clusters. Tiny particles seen in the background are single molecules of typical size 30 nm.

Thus the fractal dimension is dependent on the kinetics of the pattern formation process represented by the *z* parameter in Eq. (3). For a one-dimensional system one can solve for *z* exactly. Numerical solutions for the *z* parameter for $D\geqslant2$ has been discussed by Brilliantov *et al.* [8], and an explicit dependence of the fractal dimension on α has been shown over a wide range of α values.

The theoretical concepts recapitulated above necessitate three requirements: (i) the system has a wide size particle distribution, (ii) the fractal state is an intermediate phase, and (iii) the final state is a state where the smallest particle size ''wins,'' giving rise to a regular cluster. These conditions are sufficiently met in our experiment; thus the formalism described above is a suitable model for the analysis of the following experimental results.

The AFM pictures taken at titration points corresponding to ethanol concentration $=0\%$ (v/v) and 45% (v/v) were very revealing. Figure 1 shows the size distribution of gelatin molecules and small aggregates of various sizes dispersed in the solution in the absence of ethanol. Particles of sizes $\approx$65, 190, and 380 nm are clearly visible in the presence of larger aggregates and tiny particles, indicating a large polydispersity in size and shape. The corresponding particle size distribution (Fig. 2) was estimated from dynamic light scattering (Brookhaven Instruments, USA) and the wide particle size distribution is consistent with the requirement of Eq. (1) and least-squares fitting, yielding $\alpha=4.01$. At ethanol concentration $\approx45\%$ (v/v) the AFM scan taken from two different surfaces yielded micrographs shown in Figs. 3(a) and 3(b). One observes beautiful fractal trees with branches emerging from large aggregates. There is a swarm of small particles and a 650-nm aggregate near one end of these trees in Fig. 3(a). Interestingly in the close vicinity of these fractal trees no free particles are present, implying the participation of all smaller gelatin aggregates available in that space in the formation of the fractal structures. The swarm of approximately 200-nm size particles seen is plausibly in the process of joining the fractal tree or starting a new structure from the 1300-nm cluster available nearby. Figure 3(b) shows neither a direction dependent affinity nor an isotropic self-similarity, though in Fig. 3(a) a direction dependent affinity is clearly seen.

The stochastic self-similarity and scaling of the random fractals observed in Figs. 3(a) and 3(b) was ascertained from the fractal dimension, d_f. This is defined as [17]

$$d_f(s)=\lim_{\varepsilon\to0}\frac{\ln M(\varepsilon)}{\ln(1/\varepsilon)}, \tag{4}$$

where *s* is a subset of *N*-dimensional space occupied by the fractal object and $M(\varepsilon)$ is the number of *N*-dimensional cubes required to cover the subset *s*. Our analysis yielded $d_f=1.60\pm0.05$ for Fig. 3(a) and 1.58 ± 0.05 for Fig. 3(b). Except in the case of mica the formation of fractal aggregates with identical D_f values were observed on all other surfaces, implying the universality of surface adsorbed dynamics of gelatin aggregation. The self-similarity of the fractals could be established over five decades of the length scale, as shown in Fig. 4. For illustrating self-similarity of gelatin aggregates, we have shown two AFM pictures, one with a 10-μm scan and another with a 95-μm scan, both yielding the same fractality. The fractal aggregates formed under stringent preparation protocols. No fractal aggregates could be formed when both ethanol and salt were absent in the solution. Again the fractal aggregates were observed only in a extremely narrow range of ethanol concentration $[=(45\pm2)\%]$ in all cases.

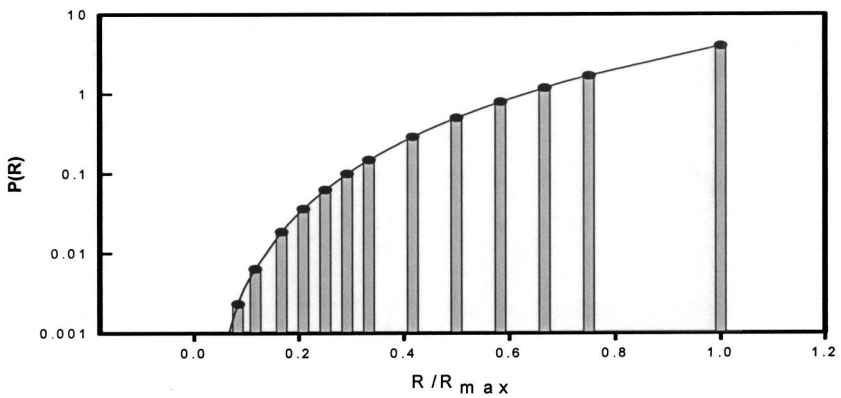

FIG. 2. Dynamic light scattering measurement of the particle size distribution of the same sample as in Fig. 1. Fitting to Eq. (1) gives $\alpha=4.01$.

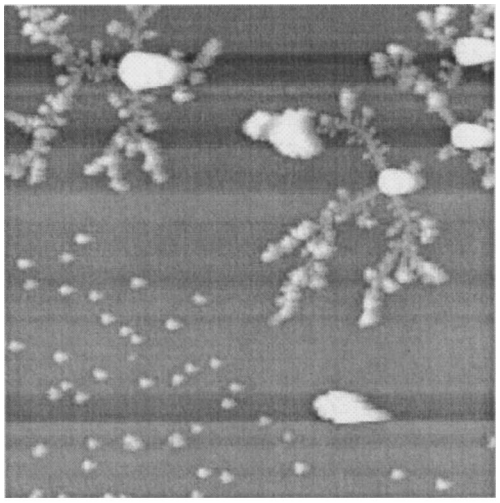

(a)

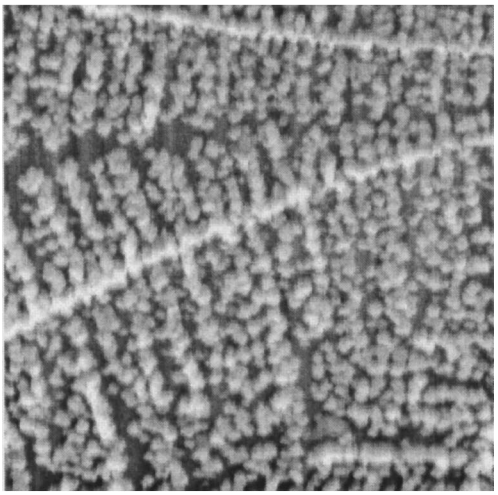

(b)

FIG. 3. (a) Scanning probe micrograph ($10\times10\ \mu m^2$) of the solution adsorbed on a glass substrate having an ethanol concentration of $\approx45\%$ (v/v). The fractal trees are seen to emerge from 1300-nm clusters. Swarm of free particles (size ≈200 nm) are seen along with a 1300-nm aggregate, which are yet to join to form another fractal tree. Notice the propensity of directional affinity and the absence of isotropic self-similarity; the fractal arms have $d_f=1.60\pm0.5$. (b) Scanning probe micrograph ($95\times95\ \mu m^2$) of the solution adsorbed on a silicon substrate having an ethanol concentration of $\approx45\%$ (v/v). Notice that the assembly has a more isotropic self-similarity as compared to Fig. 3(a), though both have the same $d_f=1.58\pm0.5$.

In the RSA model, a fractal dimension of 1.6 will yield a value for the spatial correlation term $\alpha\approx4$ self-consistent with the result of fitting of Eq. (1) to the DLS particle size distribution, and a spatial coverage term $z\approx0.07$ [8]. Consequently, the fraction of the uncovered area would decrease with time t following the power law $\sim t^{-0.07}$ which would result in a reduction of the typical gap between two neighboring adsorbed particles following the power law $\sim t^{-0.2}$. The measured $d_f=1.6$ is close to the theoretical value for the fractal dimension of DLA clusters ($=1.7$ in $D=2$) implying

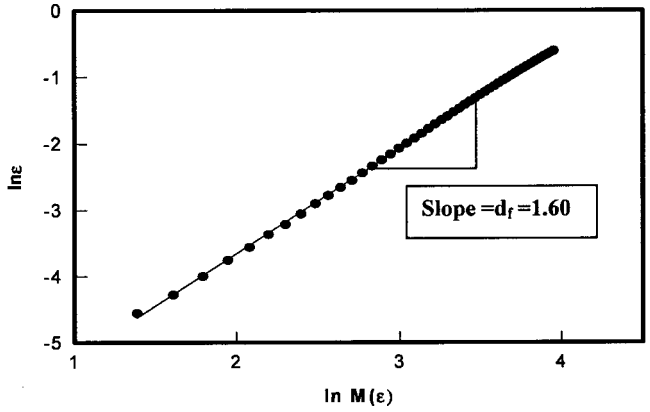

FIG. 4. Double-logarithmic plot of $N(\varepsilon)$ vs $1/\varepsilon$ for the gelatin aggregates shown in Fig. 3(a) for the aggregates formed on glass substrate. The fractal dimension is deduced from the slope.

that the aggregation dynamics was driven by a diffusion process. The experiments were performed at pH=5 very close to the isoelectric pH of gelatin ($=4.9$) where the individual molecules carried nearly a zero net charge, which only confirms zero electrophoretic mobility. However, this does not preclude electrostatic interactions between positive and negative charged segments of same or different gelatin molecules leading to aggregation.

Ethanol evaporates selectively and slowly, giving rise to a solvation instability because of which, for example, a fully solvated molecule or aggregate finds itself suddenly devoid of a solvation layer either partially or fully. The available solvent reorganizes to provide optimum solubility to all the gelatin aggregates, which leads to a reorganization inside the aggregates leading to morphological changes at the macroscopic level. In order to study this, these fractal structures were allowed to evolve with time for several days, and we obtained AFM pictures taken after seven days as shown in Fig. 5, where one clearly sees more regular structures that

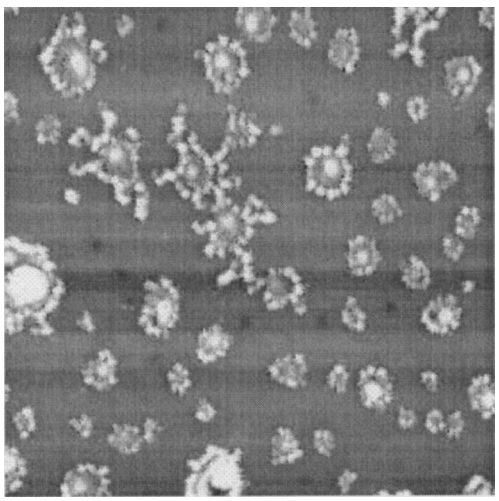

FIG. 5. Scanning probe micrograph ($10\times10\ \mu m^2$) of the same sample as in Fig. 3(a) after seven days. Notice the popcorn shaped aggregates, which typically have 500-nm aggregates at the core. The corona has a fractal dimension $d_f=1.59\pm0.5$.

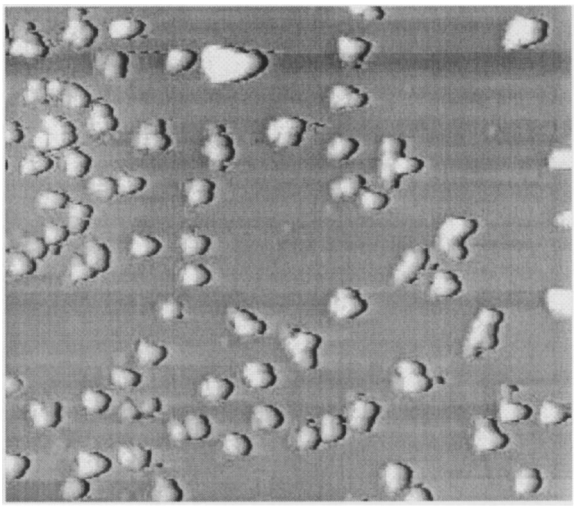

FIG. 6. Scanning probe micrograph ($10\times10\ \mu m^2$) of the same sample as in Fig. 3(a) after 14 days. Notice that the popcorn shaped aggregates seen earlier in Fig. 5 have melted to give rise to typically 500-nm aggregates all over.

look like popcorn tunnels with fractal coronas of a core size of 500 nm. The fractal dimension of the corona was $d_f = 1.59 \pm 0.5$ not very different from that of the fractal aggregates seen initially. After about 14 days, the AFM image of the structure appears as shown in Fig. 6. All the fractal structures have disappeared, giving rise to near-spherical aggregates of a typical size 500 nm qualitatively. But the 650- and 1300-nm clusters, that served as bases of these trees, are still present minus their fractal arms. These features were observed universally on hydrophilic surfaces like glass, silicon, and quartz for both Sigma and Merck gelatin samples where, as a hydrophobic surface, mica did not support the formation of such clusters.

The d_f values obtained were not very different from that of DLA clusters though it appears that sometimes [see Fig. 3(a)] seeding particles are present on the surface that provide nucleation sites for growth. However such seeding particles were not observed in other AFM pictures [see Fig. 3(b)]. We believe that our system is closer to RSA because (i) it has followed Brilliantov *et al.*'s [8] RSA dynamics faithfully, (ii) DLA produces smaller aggregates of low polydispersity where as in our case the aggregate size and polydispersity were both large, and (iii) DLA clusters exhibit a direction dependent affinity which was not observed universally. On the contrary, isotropic self-similarity is not shown by DLA whereas most of our fractal aggregates did so.

B. Growth of aggregates in bulk

Smoluchowski aggregation kinetics, which is a versatile and powerful tool to model aggregation phenomenon, has been successfully used to describe the time-dependent evolution of aggregate size in biopolymeric systems [4]. In an earlier work [9] involving the sol-gel transition in aqueous gelatin solutions, the Smoluchowski aggregation kinetics adequately described the temporal growth of gelatin under going a gel transition. In this model, the temporal evolution of size distribution $n_i(\tau)$ is given by

$$\frac{dn_k}{d\tau} = \sum_{i+j=k=2}^{\infty} n_i A_{ij} n_j - 2\sum_{j=1}^{\infty} n_k A_{kj} n_j . \tag{5}$$

Here, the reduced time τ is defined through a collision rate constant (γ_s) as $\tau = \gamma_s \varepsilon t$. Smoluchowski assumed that the i-mer and j-mer bind irreversibly on collision and the probability of their collision is given by ε (also called sticking coefficient). The transition matrix A_{ij} is given as

$$A_{ij} = \frac{(D_i + D_j)(R_i + R_j)}{4D_0 R_0}. \tag{6}$$

Smoluchowski assumed $A_{ij} \approx 1$ and came up with a cluster size distribution as function of time τ as

$$n_i = \frac{\tau^{i-1}}{(1+\tau)^{i+1}}, \quad i = 1,2,3.... \tag{7}$$

In this picture, the clusters grow with a power law behavior where the radius of ith cluster (a cluster with i monomers in it) will show $R_i \sim i^{\beta}$ with $\beta = 1/d_f$. The cluster exponent $\beta = 1/3$ for spherical closely packed cluster, 1/2 for a linear random coil polymerlike cluster and $6/5D$ for diffusion limited clusters, where D is the Eucleadian dimension.

The intensity of the light scattered from such a system will be

$$I_s = I_0 \sum_i n_i i^2, \tag{8}$$

and the same for radius of the aggregate will be given as

$$R_h^2 = \sum_i n_i R_i^2 i^2. \tag{9}$$

Where R_0 and I_0 are radius of the monomer and intensity of light scattered by a monomers in solution. Equations (8) and (9) with Eq. (7) will yield

$$I_s = I_0(1 + 2\tau) \tag{10}$$

and

$$R_h = R_0(1 + \tau). \tag{11}$$

A more generalized approach gives

$$I_s = I_0(1 + \Gamma_I \tau)^{\delta_I} \tag{12}$$

and

$$R_h = R_0(1 + \Gamma_R \tau)^{\delta_R}, \tag{13}$$

where Γ_I and Γ_R are the intensity and radius growth rate parameters. δ_R can be approximated to the cluster exponent $\beta = 1/d_f$. However for δ_I no such clear relationship can be established.

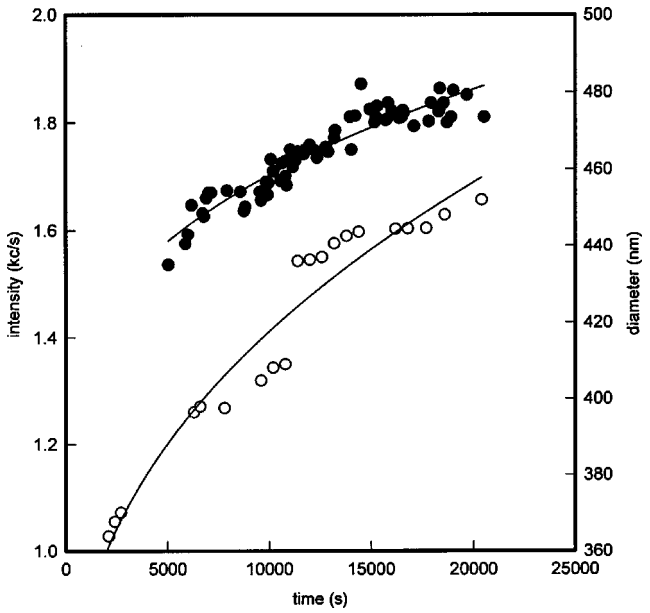

FIG. 7. Temporal growth of effective diameter $R_h(t)$ (○) and intensity (●) of light $I_s(t)$ scattered from aggregated gelatin molecules in aqueous solutions measured by dynamic light scattering. The data fitting to $R_h(t) \sim I_s(t) \sim t^{1/d_f}$ gave $d_f = 2.6 \pm 0.2$.

The temporal growth of aggregates in the bulk of the solution was measured through intensity of light scattered (I_s) at 90° and effective hydrodynamic radius R_h. The variations are shown in Fig. 7. The corresponding polydispersity (P) that characterizes the width of the particle size distribution is shown in Fig. 8. The experimental data could not be fitted to Eqs. (12) and (13), if we follow the data treatment alike in Ref. [9]. In fact, the temporal growth of hydrodynamic radius $R_h(t)$ and scattered intensity $I_s(t)$ measured in the bulk were observed to exhibit $R_h \sim t^z$ and $I_s \sim t^z$, with $z = 1/d_f$, giving a fractal dimension d_f in $3D \approx 2.6 \pm 0.2$. Based on this, one can argue that in Eqs. (12) and (13) the second term in the bracket is the dominant term ($\Gamma_R \tau$ and $\Gamma_I \tau \gg 1$) giving the observed power-law features to measured R_h and I_s versus t data. A second inference is that though Smoluchowski

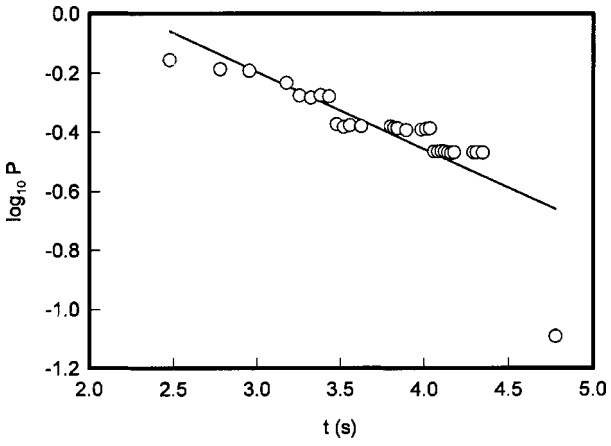

FIG. 8. Temporal variation of the polydispersity parameter P of aggregated gelatin molecules in aqueous solutions measured by dynamic light scattering. The data fitting yielded $P \sim t^{-0.2}$.

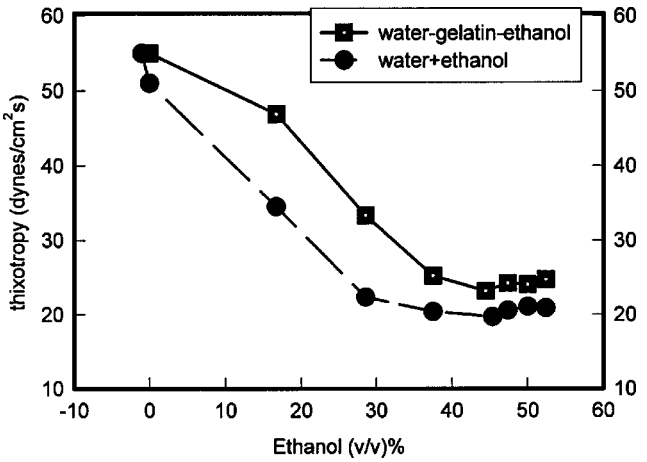

FIG. 9. Variation of the solution thixotropy as a function of the ethanol concentration for aqueous solutions with the without gelatin. Notice that the presence of ethanol increases the solution thixotropy significantly.

aggregation model adequately describes the gelation kinetics in this biopolymer (Ref. [9]) its applicability to self-association remains rather qualitative.

For the present system, the scattering wave vector, q that defines reciprocal of the probe length scale, implies that $q\,R_h \approx 1$. Hence, we are not deep inside the Porod regime and would liberally interpret our light scattering data within the Guinier scattering model frame work. In this domain, the aggregates scatter as the square of their mass m, and for fractal objects R_h determines noninteger moments of the aggregate distribution. Thus [18]

$$I_s \sim \langle m^2 \rangle / \langle m \rangle, \tag{14}$$

$$R_h \sim \langle m^2 \rangle / \langle m_f^{(2-1/d)} \rangle. \tag{15}$$

If one assumes scale invariance of aggregate distribution, Eqs. (14) and (15) reduce to

$$I_s \sim \langle m \rangle, \tag{16}$$

$$R_h \sim \langle m \rangle^{1/d_f}, \tag{17}$$

leading to $R_h \sim \langle I_s \rangle^{1/d_f}$, consequently a plot of $\log R_h$ against I_s should yield the fractal dimension of the cluster, which was not observed in our case implying absence of such scale invariance in aggregate size distribution.

The polydispersity parameter (P) deduced from the normalized second moment [16] of the correlation function, showed a remarkable decrease with time (Fig. 9), implying that larger aggregates were selectively formed at the cost of smaller ones alike, as was seen on the substrates. The temporal dependence exhibited, $P \sim t^{-0.2}$. During the association process, the highly polydisperse aggregates are driven towards a close to monodisperse solution. DLA processes are known to produce smaller aggregates formed rapidly with a wide particle size distribution. In contrast RCA aggregates

grow slowly into large clusters and exhibit a low polydispersity in size distribution. The fractal dimension observed in the bulk (d_f in $3D \approx 2.6 \pm 0.2$) is close to that of the DLA whereas the polydispersity feature and aggregate size growth mimics that of a RCA process, which appears anomalous.

The physical mechanism of aggregation in the bulk can be visualized as follows. Gelatin is not soluble in alcohols whereas water is a good solvent. As ethanol is added to water, the water molecules will preferentially bind to the alcohol molecules through hydrogen bonding (we will see this more explicitly in Sec. III C) and the resultant binary mixture becomes a marginal solvent for gelatin molecules. Second, the dielectric constant (ε) decreases [19] significantly, facilitating stronger electrostatic interactions between charged segments (both intra and inter) of gelatin molecules. The strength of electrostatic interactions between two oppositely charged particles increases as $\varepsilon^{-3/2}$ at a given temperature as per the Debye-Huckel theory [20]. Since the solution pH was close to the isoelectric point of gelatin, there is no net charge on the polypeptide. Nonetheless, as mentioned already, the chemical structure of this biopolymer indicates almost a 1:1 positive and negatively charged patches on this linear random coil molecule. These overlap as the chain contracts due to the decrease in the Flory-Huggin solute-solvent interaction [21] brought in by the presence of ethanol, resulting in bringing charged segments to each other's vicinity through electrostatic interactions yielding chain collapse.

C. Rheology of the solution

Structure evolutions (disintegration and reformation of structures) are not instantaneous, which gives rise to thixotropy. There are several model methods to evaluate the thixotropy parameter for a given complex fluid. The rheology data were fitted to Herschel-Bulkley, Cross, power law, and Carreau models [22], but the model that provided the best data fitting was Cross model, defined as

$$\frac{\eta - \eta_\infty}{\eta_0 - \eta_\infty} = \frac{1}{1 + (c\dot{\gamma})^d},$$

where η_0 and η_∞ indicate zero and infinite shear rate viscosities, c is a consistency coefficient, and d is the rate index. However, the Cross and Herschel-Bulkley models gave identical thixotropy values. The software provided by T. A. Instruments, UK was used for all the data analysis reported here.

The thixotropy evaluated from shear stress versus shear strain data is plotted as a function of ethanol concentration in Fig. 10, which reveals shear thinning or pseudoplastic fluid features. The thixotropy of the ethanol-water binary mixture decreases with increased ethanol concentration and reaches a minimum at an ethanol concentration $\approx 45 \pm 3\%$ v/v. Beyond this, the thixotropy value rises again. When gelatin was added as a third component the thixotropy fell by typically 20% of its value compared to that of ethanol-water binary mixture value. Regardless, the minimum was still located at an ethanol concentration $\approx 45 \pm 3\%$ v/v.

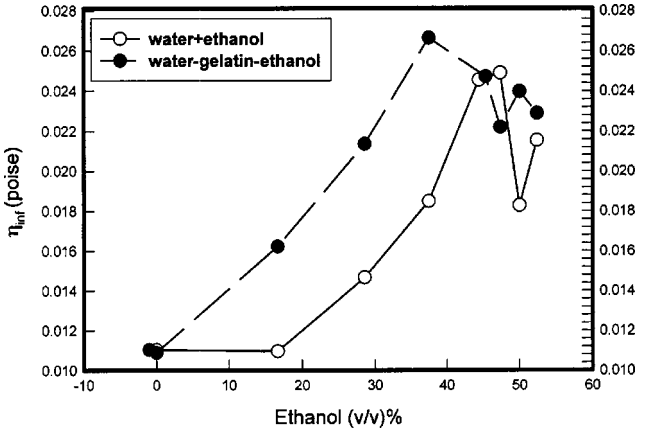

FIG. 10. Variation of the solution viscosity at infinite frequency as a function of the ethanol concentration for aqueous solutions with and without gelatin. Notice that the presence of ethanol increases the solution thixotropy significantly, and close to an ethanol concentration of $\approx 45 \pm 2\%$ v/v there is a dip in the viscosity value. This is the region where fractal aggregates are formed on hydrophilic substrates.

The viscosity versus shear rate plot is given in Fig. 11 for various ethanol concentrations, which again exhibits pseudoplasticity. Shear thinning, which is the essential feature of many complex fluids, is clearly seen here, and this arises from the elongation of the structures along the direction of the shear. η_∞ of the ethanol-water binary mixture increases with increased ethanol concentration and reaches a maximum at an ethanol concentration $\approx 45 \pm 3\%$ v/v. Beyond this, the η_∞ value falls. When gelatin was added as a third component η_∞ increased by typically 50% of its value compared to that of ethanol-water binary mixture value. Regardless, the maximum was still located at an ethanol concentration $\approx 45 \pm 3\%$ v/v.

The rate index parameter d that defines the sharpness of viscosity change typically varied in the narrow range 0.6–

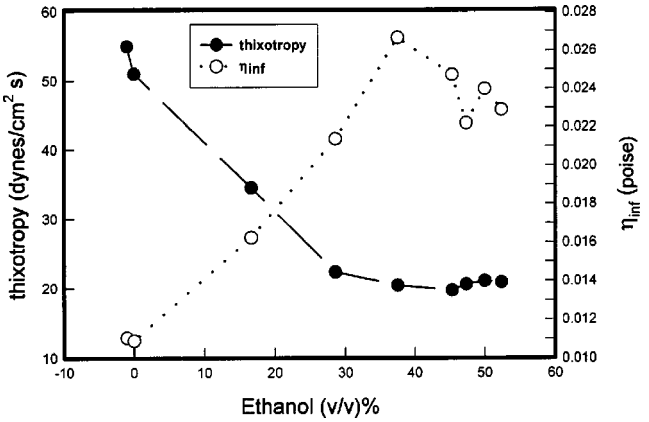

FIG. 11. Comparison of the solution viscosity at an infinite frequency as a function of the ethanol concentration for aqueous gelatin solutions. Notice that the solution thixotropy rises close to an ethanol concentration of $\approx 45 \pm 2\%$ v/v, where there is a dip in the viscosity value. This is the region where fractal aggregates are formed on hydrophilic substrates.

0.8 for all the solutions regardless of the presence of gelatin (for pure water $d \approx 0.75$). The consistency coefficient c on the other hand, remained close to 3.5 for solutions (which is the pure water value) with gelatin whereas for water-ethanol mixtures the same was an order of magnitude larger. This implies that the presence of ethanol does change viscoelastic nature of the solution rather significantly.

The infinite shear rate viscosity (η_∞) was found to be very sensitive to ethanol concentration and this is shown in Fig. 10 along with the corresponding thixotropy values. Note that close to ethanol concentration $\approx 45 \pm 2\%$ v/v, thixotropy shows a minimum whereas η_∞ shows a maxima. We could not obtain reproducible zero shear rate viscosity (η_0) values. Since gelatin molecules are several orders of magnitude larger in size than ethanol molecules, energetically hydrogen bonding between ethanol and water will be more favorable. This results in the formation of hydrogen bonded ethanol-water clusters that support a thixotropic behavior. It is plausible that at this specific concentration of ethanol, the stoichiometric condition for maximum hydrogen bonding between alcohol and water molecules is achieved. The observed thixotropy reflects the disintegration and reformation of such hydrogen-bonded ethanol-water structures.

IV. CONCLUSION

It has been shown that the binary liquid mixture of ethanol and water exhibit maximum hydrogen bonding at ethanol concentration $\approx 45 \pm 2\%$ v/v which is supported by thixotropic and viscosity data. This provides the appropriate thermodynamic environment for the gelatin molecules to form self-assembled clusters of fractal dimension ≈ 2.6 in the bulk (3D) and 1.6 on surfaces (2D). We have proposed a RSA model for surface aggregation of gelatin because of the following reasons. Exposing a surface to a polymer solution (polydispersity assumed) containing absorbable polymer molecules and aggregates creates an instantaneous nonequilibrium situation. Thermodynamically, the larger particles have a higher surface affinity because they make more surface contact per molecule. Since the free energy of hydration is also negative, larger particles on the surface are preferred. However, due to their higher diffusion coefficients smaller particles will reach the surface first and there will be a propensity of these initially on the substrate. Once these reach the surface there is kinetic rearrangement of the particles to minimize the total surface free energy of the adsorbed solution layer. At equilibrium the smaller particles are desorbed and coalesce into larger particles to minimize the free energy of hydration. In the present case, the selective evaporation of ethanol expedites this process and various microstructures evolve with time. The size polydispersity imparts randomness to the whole process, which is a necessary condition for RSA. Above constitutes a generalized description of RSA model [5,6], and this is exactly what was observed in our 2D experiments. Specifically, the fractal aggregates formed on hydrophilic surfaces followed random sequential adsorption kinetics with the initial particle size distribution given by a power law. These aggregates followed a sequence of morphological time dependent changes, driven by selective but slow evaporation of ethanol, to yield several types of self-organized aggregates. Surface tension does play a role here, which needs to be explored. The aggregation in the bulk of the solution appears to be an anomalous process and could be explained through a Smoluchowski aggregation model, albeit qualitatively. It gives a DLA type fractal dimension to the cluster but shows an extremely low polydispersity, which in fact is a signature of a slowly growing RCA aggregate. The coherent picture that emerges is as follows. (i) At this specific alcohol-water mixture, the hydrogen bonding between the two liquids is at its maximum. (ii) Since such a solvent is a marginal one for gelatin, which is a linear random coil polymer, the charged segments of this polyampholyte overlap due to electrostatic attractions leading to contraction of the chain. This can be both intermolecular or intramolecular, which results in the formation of fractal aggregates. In the bulk this produced aggregates of narrow particle size distribution. (iii) The morphological evolution of aggregates on hydrophilic surfaces owes its origin to selective evaporation of ethanol, that leads to solvation instability of the gelatin molecules and the concomitant optimization of sharing of the available solvent.

[1] H. G. Bungenberg de Jong, in *Colloid Science,* edited by H. R. Kruyt (Elsevier, New York, 1949), Vol. II, p. 335

[2] A. I. Oparin, *The Origin of Life on Earth* (Oliver and Boyd, London, 1957).

[3] T. A. Witten, Jr. and L. M. Sander, Phys. Rev. Lett. **47**, 1400 (1981); Phys. Rev. B **27**, 5686 (1983).

[4] J. Feder, T. Jossang, and E. Rosenqvist, Phys. Rev. Lett. **53**, 1403 (1984); J. Chem. Phys. **82**, 574 (1985).

[5] J. W. Evans, Rev. Mod. Phys. **65**, 1281 (1993).

[6] Pablo Jensen, Rev. Mod. Phys. **71**, 1695 (1999).

[7] A. DiBiasio, G. Bolle, C. Cametti, P. Codestefano, F. Sciortino, and P. Tartaglia, Phys. Rev. E **50**, 1649 (1994).

[8] N. V. Brilliantov, Y. A. Andrienko, P. L. Krapivsky, and J. Kurths, Phys. Rev. Lett. **76**, 4058 (1996).

[9] H. B. Bohidar and S. S. Jena, J. Chem. Phys. **98**, 8970 (1993).

[10] H. B. Bohidar and S. S. Jena, J. Chem. Phys. **100**, 6888 (1994).

[11] A. Veis, *The Macromolecular Chemistry of Gelatin* (Academic Press, New York, 1964).

[12] E. Kokufuta, Prog. Polym. Sci. **17**, 647 (1992).

[13] D. J. Burgess and J. E. Carless, Int. J. Pharm. **27**, 61 (1985); M. Tsung and D. J. Burgess, J. Pharm. Sci. **86**, 603 (1997).

[14] D. J. Burgess and G. N. Singh, J. Pharm. Pharmacol **45**, 586 (1993).

[15] W. Lin, Y. Zhou, Y. Zhao, Q. Zhu, and C. Wu, Macromolecules **35**, 7407 (2002).

[16] H. Z. Cummins and E. R. Pike, *Photon Correlation and Light Beating Spectroscopy* (Plenum Press, New York, 1974).

[17] K. S. Birdi, *Fractals in Chemistry, Biochemistry and Biophysics* (Plenum Press, New York, 1991).

[18] J. G. Rarity and P. N. Pusey, in *On Growth and Forms*, edited by H. E. Stanley and N. Otrowsky (Martinus Nijhoff, Boston, 1986), p. 218.
[19] R. Waller and T. J. K. Strang, Collection Forum **12**, 70 (1996).
[20] C. Tanford, *Physical Chemistry of Macromolecules* (Wiley, New York, 1967).
[21] P. J. Flory, *Principles of Polymer Chemistry* (Cornell University Press, Ithaca, NY, 1953).
[22] H. A. Barnes, *Handbook of Elementary Rheology* (University of Wales Press, UK, 2002).